A More Flooding-Tolerant Oxygen Electrode in Alkaline Electrolyte

M. B. Ji, Zidong Wei, S. G. Chen, Q Zhang, Y.Q. Wang, X. Q. Qi, L. Li

Fuel Cells

A More Flooding-Tolerant Oxygen Electrode in Alkaline Electrolyte

Journal:	*Fuel Cells*
Manuscript ID:	FUCE.200800150.R3
Wiley - Manuscript type:	Original Research Paper
Date Submitted by the Author:	13-Dec-2009
Complete List of Authors:	JI, M. B. WEI, Zidong; Chongqing Univ., Chemistry CHEN, S. G. ZHANG, Q Wang, Y.Q. QI, X. Q. LI, L.
Keywords:	AIR ELECTRODE, Alkaline Fuel Cell, FLOODING, METAL/AIR BATTERY, WATER MANEGEMENT

A More Flooding-Tolerant Oxygen Electrode in Alkaline Electrolyte

M. B. Ji[1,2], Z. D. Wei*[1,2], S. G. Chen[2], Q. Zhang[1,2], Y. Q. Wang[2], X. Q. Qi[1,2], L. Li[1,3]

[1]State Key Laboratory of Power Transmission Equipment & System Security and New Technology, School of Chemistry and Chemical Engineering, Chongqing University, Chongqing, 400044; China

[2]School of Material Science and Engineering, Chongqing University, Chongqing, 400044; China

*Corresponding author's E-mail: zdwei@cqu.edu.cn (Wei), Tel: +86 23 60891548, Fax: +86 23 65106253.

Abstract

Owing to the inherent performance and cost advantages alkaline fuel cells (AFC) have been being a highlight in fuel cells research. However the degradation of the performance coming from the cathode due to the oxygen diffusion limit leaded by the flooding is a critical issue to overcome. The objective of this study is thus devoted to mitigate the water flooding happening in the pores of a porous oxygen electrode by using a more flooding-tolerant electrode (FTE) which contains water-proof oil, dimethyl-silicon-oil (DMS). The FTE performance was checked in two cases, the whole FTE completely immersed in 1 mol L^{-1} KOH, and its catalyst layer side exposed to 1 mol L^{-1} KOH but its back side to gas chamber, in order to simulate the situation of electrode flooded and electrode at normal operation condition, respectively. The results indicate that the FTE displays outstanding flooding-tolerant capability, especially in the case of a large current density, in which mass transport of gas reactant is in a dominant position.

Key Words: flooding-tolerant, AFC, metal/air batteries, water flooding, water-proof oil

1. Introduction

Fuel cells allow an environmentally friendly and highly efficiently conversion of chemical energy to electricity. Therefore, they have a high potential to become important components of an energy-efficient and sustainable economy. The main challenges in the development of fuel cells are cost reduction and long-term durability [1]. In recent years, there has been the reemergence of interest in alkaline fuel cells (AFCs), as the development of low cost polymer electrolyte membrane fuel cells (PEMFCs) took much more efforts than expected [2,3]. Whereas the cost can be significantly reduced by the use of non-noble and less costly catalysts [3-5] for the faster oxygen reduction kinetics in liquid alkaline electrolyte over acidic media, the poor lifetime, mainly due to the hydrophobic area of the gas diffusion electrode flooded by water and electrolyte, desiderates to be overcome, which has become the decisive factor for their commercialization [6]. In practical applications, not more than 5000 operating hours [3] could be obtained. It is obvious that most efforts of any research group dealing with AFCs is not to decrease the cost as the cost is low compared to other fuel cell systems anyway, but to increase the lifetime [2], especially for the oxygen electrode (i.e. the cathode of AFCs and metal/air batteries).

Gas diffusion oxygen electrodes, where molecular oxygen is reduced, are vital to AFCs and metal/air batteries performance. As shown in Figure 1, the oxygen reduction reaction (ORR) takes place in the three-phase zone formed by the catalyst, the electrolyte and reactants. For the transport of the oxygen to the three-phase zone in the electrodes and the transport of OH^- ions out of the electrodes a porous structure is needed, whereby a hydrophilic pore system is required for the transport of water with hydroxide group and a hydrophobic pore system for the transport of the oxygen or air. Therefore, the balance of

hydrophobic and hydrophilic properties of the materials determines the operation conditions and the electrochemical performance. For the stability of the output performance, it is necessary that hydrophobicity does not change during the fuel cell operation. Generally, polytetrafluoroethylene (PTFE) is used to provide a hydrophobic character to the electrodes and the hydropobicity of the electrodes is adjusted by the concentration of the PTFE [7, 8]. In principle, PTFE is not only strongly hydrophobic, but it has a very high stability in aggressive chemical environmental conditions. However there are many investigations have observed the decomposition [1,3,6,7,9,10] and partial removal [7,11,12] of PTFE during both the AFCs and metal/air batteries operation, which reduces the hydrophobic property and results in the excessive oxygen electrode wettability. As a result, the built up of liquid electrolyte in the gas pores prevents the efficient diffusion of oxygen to the reactive sites and also reduces the effective area of the three-phase gas–solid–liquid interface, thereby leading to the final flooding of the oxygen electrode [13] as shown in Figure 1.

Moreover, as the current demand increases during operation, it is believed that the reaction front moves outward toward the air side of the electrode, and more of the electrode surface area participates in the reaction. The liquid electrolyte would film over or flood the electrode surface, thereby blocking oxygen access and reducing the active (available) three-phase interfacial area for reaction [14]. Besides, the imperfections in the wet proofing coating in which the pressure of the static KOH (5-10 kPa over ambient) forces the KOH into the dry pores can lead to a slow and constant physical flooding phenomenon [3].

Indeed the negative impact of carbon dioxide on the porous structure of the oxygen electrode is also an unavoidable factor if the system uses air as the oxidant instead of pure

oxygen. As the result of poisoning reaction of carbon dioxide and alkaline electrolyte the formation of carbonate may precipitate and block the micro pores and thus limit the gas diffusion inside the catalytic layer to the active sites. The phenomenon will be more serious at lower temperature [15] and in higher concentration electrolyte [3, 16]. Thus the carbonate precipitation in the porous system significantly enhances the ‘‘flooding’’ of the gas electrode and interferes with the electrode kinetics, affects the durability and activity of gas diffusion electrodes.

The most common method to alleviate the negative influence of carbon dioxide is the use of chemical scrubbers, (i.e. soda lime [2, 3, 17-21]) or regenerative scrubbers, which function on the principles of pressure-swing adsorption, temperature-swing-absorption, and the steam-regeneration of amines [3] for scrubbing CO_2 from the air-stream. But this is cumbersome and comparatively costly not a strong option for commercial systems [21].

The net result of all cathode flooding phenomena is that the supply of oxidant to the system lags behind the demand causing a shortage of oxygen and possible local starvation of oxygen for the reaction thus increasing the concentration overpotential of the cathode. Worse still, the oxygen electrode cannot sustain the current density from the stack, resulting in premature battery failure and the final cell reversal [2]. As long as the cell reversal appears, the output and mechanical damage of the stack and the electrode will be seriously impaired. In order to make the oxygen electrode more resilient to the effect of flooding, the current methods include improving the waterproofing of the electrode via the use of more hydrophobic carbons [13], binary carbon supports [22, 23], more PTFE [24-26], and appropriate heat treatments of the finished electrodes [3]. However, higher PTFE loading

increases the resistance and decreases the performance of the cell [27], besides the denaturing of the PTFE binder with time is an irreversible degradation process. Moreover, the reduction of the electrode surface area and the increase in the wetting of the electrode is also a function of hours the electrode is operated [28].

So it very important to design a gas diffusion oxygen electrode with stabile three phase interface that electrolyte can penetrate into but not over-flood. The objective of this study is thus devoted to mitigate the flooding problem with the development of a novel oxygen electrode containing water-proof oil, dimethyl-silicon-oil (DMS), which was added into parts of cathode pores of the conventional MnO_2/C electrode. The solubility of oxygen in DMS is over 10 times higher than that in water. Thus, the pores occupied by DMS form permanent channels for oxygen transportation, in which the DMS is not easily extruded by water, no matter whether the cathode is flooded or not. The channels for oxygen transportation and OH^- ions are orderly allotted between the channels/pores occupied by DMS and electrolyte, respectively, with the addition of the water-proof oil DMS as shown in Figure 1, where the oxygen and OH^- hold their own fixed and stabile transport channels, respectively. Because carbonate precipitation only happens in the alkaline aqueous phase rather than in the water-proof oil phase, we suppose that the addition of DMS may alleviate the electrolyte carbonation. The electrode containing such water-proof oil is called flooding-tolerant electrode (FTE) hereafter. The electrode without such water-proof oil is named a conventional MnO_2/C electrode (CME) for the sake of contrast.

2. Experimental

2.1 Preparation of the FTE

The catalyst 7 wt.% MnO_2/C was obtained by calcining the mixture of SL-30 carbon black (Zigong carbon black, China), $Mn(NO_3)_2$ at 340 °C for 0.5 h according to the method reported in Reference [29]. Conventional MnO_2/C electrode (CME) was composed of a gas diffusion layer and a catalyst layer. The gas diffusion layer was prepared on wet-proofed carbon paper as described in Reference [12]. In short, The carbon powder (Vulcan XC-72, Cabot Corp.), 30 wt.% of PTFE and ethanol was ultrasonically mixed with a ratio 13:7 of carbon to solid PTFE loading. The viscous mixture was coated onto the wet-proofed carbon paper (Toray Co, Jap.) with PTFE and then heated at 340 °C for 30 minutes to prepare the micro-porous layer (MPL). The thickness of the carbon paper and the MPL is 260 μm and 20μm, respectively. The PTFE content in carbon paper is 40 wt.% and the loading of the carbon in MPL is 1 mg cm^{-2}. A suspension consisting of catalysts 7 wt.% MnO_2/C, 30 wt.% of PTFE and/or 0.5 wt.% Nafion solution (Du Pont) and ethanol was first ultrasonically mixed for about 15 min, respectively. The weight ratios of MnO_2/C to solid PTFE or Nafion were maintained at both 17:3. The suspension was pipetted onto the gas diffusion layer and finally heated at 340 °C and/or 145 °C, respectively. Thus the PTFE-bonded CME and Nafion-bonded CME were obtained; the latter was used to simulate the completely hydrophilic CME after decomposition or partial removal of PTFE. The MnO_2 loading was 0.5 mg cm^{-2} for all electrodes and the thickness of the catalyst layer was ca. 170 μm by estimation.

The FTE was obtained based upon the CME according to the following steps. First, the 50 vol.% DMS solution with iso-propanol as solvent was sprayed onto the catalyst side of the

above CME, and then extracted with a water pump from the opposite of the electrode to make DMS pass through the porous electrode and remove the surplus DMS under a pressure of 10 kPa. And finally, the electrode with some residues of DMS was heated at 120 °C for 5 minutes to remove the solvent used for diluting DMS. The DMS loading was calculated by weighing the mass difference of the CME before and after the DMS treatment. The DMS containing CME is the FTE. The loading of the DMS is 2.5 mg cm^{-2} for all FTE discussed in this work.

2.2 Electrochemical characterization

A FTE or CME together with an Hg/HgO reference electrode and a Pt wire counter electrode were completely immersed in 1mol L^{-1} KOH to simulate the situation of an electrode flooding. In this "completely immersed" case, the whole electrode was dipped in the electrolyte solution, i.e., the two sides, catalyst layer side and back side of the electrode, were covered by electrolyte. The active area of the immersed electrodes is 1.5 cm^2. Pure oxygen was bubbled into the electrolyte solution near the back of the electrodes during the test. Even so, the FTE electrode is only considered in partial flooding situation owing to some oxygen bubbles impinged on the cathode getting O_2 gas directly into some of the more hydrophobic pores in the electrode. The results are shown in Figures 3, 4 and 5. The performance of the FTE was tested using an Autolab PGSYAT302 instrument (IECO CHEMIE B.V., The Netherlands) with General Purpose Electrochemical System (GPES) and frequency response analysis software (FRA).

A half cell as shown in Figure 2 was employed to simulate AFCs in a real operation

situation in which the FTE or CME is served as an oxygen cathode. In this case, only the catalyst layer side was exposed to 1 mol L^{-1} KOH but its back side to gas chamber. The results are shown in Figures 6 to 13, among which Figures 9 and 10 are the results based on the self-breathing air cathode, i.e., no force was used to drive air or oxygen flow into the cathode. In the case of Figures 6, 7, 8, 11, 12 and 13 oxygen was fed at rate of at 60 mL min^{-1} by pump. In this "half immersed" case, the catalyst layer side with 1.0 cm^2 active area exposed to KOH solution while the back side of the air electrode exposed to a gas chamber connected to oxygen source fed with ambient pressure, i.e., 101.3 kPa.

All electrochemical measurements were conducted at 25 °C. Hg/HgO electrode was employed as reference electrode in measurement. However, all potentials given in this paper have been transferred to ones vs. the RHE according to the relationship of E (RHE) = E (Hg/HgO) + 0.926 V [30].

2.3 Porosity change with introduction of DMS

The change in internal structure of the CME before and after introduction of DMS was assessed using a N_2 adsorption specific surface area analyzer (ASAP2010, Micromeritics Instrument Corp., USA).

3. Criteria for selection of water-proof oil

Water-proof oil if used successfully in an AFC or metal/air battery system must meet the following requirements:

(1) Chemically inert and thermally stable;

(2) Non-polarity molecule structure. According to the principle "Like dissolves like",

oxygen will dissolve better in a non-polar solvent than in a polar solvent;

(3) Freezing point being as low as possible but flash point as high as possible, which should cover all temperature of AFC and metal/air batteries operation;

(4) A low vapor pressure over a large temperature scope to guarantee high oxygen solubility at any temperature, low or high;

(5) Low viscosity required for efficient diffusion of dissolved oxygen;

(6) Small surface tension that is helpful for the oil itself to permeate into the deep pores in a porous electrode.

There is contradiction among the above criteria, for example, macromolecule with a small molecular weight usually has a low freezing point and low viscosity but not high flash point or low vapor pressure or large surface tension , and vice versa. With hard compromise, dimethyl-silicon-oil (DMS) with mole molecular weight of 2000 g mol^{-1} comes into sight, which is a kind of transparent liquid with colorless, flavorless and nontoxic property. Its viscosity is as low as 15 mPa·s (25 °C). The concentration of dissolved oxygen in DMS is 0.168~0.190 $ml.ml^{-1}$ (101.3 kPa, 25 °C) [31], which is 10 times higher than that in 1 mol L^{-1} KOH (0.0184 $ml.ml^{-1}$) (101.3 kPa, 25 °C) [32]. Moreover, according to Henry' law, the O_2 partial pressure at a constant total pressure decreases significantly with increase of temperature and water vapor partial pressure, thus, the concentration of dissolved oxygen in water, which is directly proportional to the O_2 partial pressure in gas phase, will decreases to 0.0067 $ml.ml^{-1}$ at 80 °C [32]. While DMS vapor pressure keeps as small as ~10^{-6} k Pa in a temperature range of 0 ~ 100 °C, thus, the concentration of dissolved oxygen in DMS almost maintains unchanged in a temperature range of AFC and metal/air batteries operation. Thus,

the concentration of dissolved oxygen in DMS will be 30 times higher than in 1 mol L^{-1} KOH at 80 °C. The relatively low freezing point (-80 °C) and quite high flash point (195 °C) of DMS are also very favorable to AFC and metal/air batteries operation. The surface tension of DMS (~19 mN m^{-1}) is approximately 1/3 of that of water (~66 mN m^{-1}). It means that DMS has much better penetrability into the deeper pores than water and can bring the dissolved oxygen into the deeper pores in a porous electrode, which extends the liquid/solid interface more effective for the ORR. The loss in O_2 diffusion coefficient with substitution of DMS for water due to increase in viscosity from 1 of water to 15 mPa·s of DMS can be estimated according Wilke-Chang's equation [33]

$$D_{AB}^{0} = 7.4\times10^{-8}\frac{(\phi M_B)^{1/2}T}{\mu_B V_{bA}^{0.6}} \quad (1)$$

Where D_{AB}^{0} is diffusion coefficient of solute A in solvent B. M_B and μ_B are mole molecular weight and viscosity (mPa·s) of solvent B, respectively. T is absolute temperature (K). V_{bA} is mole volume of solute A (for O_2: 25.6 cm^3 g^{-1} mol^{-1}) at normal boiling point. ϕ is a factor associated with solvent B, which is 2.6 for water and 1 for DMS. Thus, the diffusion coefficient of oxygen is 2.1×10^{-5} cm^2 s^{-1} in water and 1.0×10^{-5} cm^2 s^{-1} in DMS at 298 K. This computed result indicates that there is a half sacrifice in oxygen diffusion coefficient for DMS compared to that in liquid water. When the catalyst layer is severely flooded, according to the flooded agglomerates model [34], the oxygen diffusion limiting current density i_l is directly proportional to the dissolved oxygen concentration $C_{O_2}^{cl}$ in water or DMS [35-37]:

$$i_l = (nF C_{O_2}^{cl} D_{cl})/L \quad (2)$$

Where D_{cl} is the oxygen diffusion coefficient in solution of the catalyst layer; L is the

thickness of the catalyst layer; the dissolved oxygen concentration $C_{O_2}^{cl}$ and diffusion coefficient D_{cl} are 8.43 ×10^{-7} mol cm^{-3} and 1.43×10^{-5} cm^2 s^{-1} in 1 mol L^{-1} KOH solution [36] and 7.77 ×10^{-6} mol cm^{-3} and 1.0×10^{-5} cm^2 s^{-1} in DMS [31] at 25 °C and 101.3 kPa, respectively. Thus, based upon the above numbers the calculated oxygen diffusion limiting current densities vs the effective diffusion thickness *L* in liquid phase of the catalyst layer (170 μm) are listed in the Table 1. The effective diffusion coefficient is corrected by multiplying void-volume fraction, generally, 50 % for the catalyst layer. From Table 1, regardless the effective diffusion thickness *L* in liquid phase of the catalyst layer, we get at least 6.6 times higher oxygen diffusion limiting current densities with substitution of DMS for KOH solution at 25 °C. Such an increase in limiting current densities will be further strengthened at a temperature greater than 25 °C due to the decrease of dissolved oxygen concentration in higher temperature KOH solution. For example, at 80 °C and 101.3 kPa, the dissolved oxygen concentration $C_{O_2}^{cl}$ is only 3.0 × 10^{-7} mol cm^{-3} in 1 mol L^{-1} KOH solution [32], but in DMS maintains nearly 7.77 ×10^{-6} mol cm^{-3} as same as that at 25 °C. Thus, in the case of 80 °C operation temperature, the oxygen diffusion limiting current density will be enhanced to at least 18 times with substitution of DMS for KOH solution. Furthermore, the AFC is mostly operated at 80 °C. Therefore, the novel FTE with DMS will play a significant role for an AFC in application. The effective diffusion thickness *L* in the liquid phase of the catalyst layer estimated according to the data disclosed in Figures 3 to 10 is in a range of 1 ~2 μm. It means the electrodes discussed in this work are only partially flooded by electrolyte even though they were completely immersed into the electrolyte as compared with the total thickness 170 μm of the catalyst layer. As a matter of fact, we can not completely

impede some O_2 gas directly getting into some of the more hydrophobic pores owing to some oxygen bubbles impinging on the cathode. The severe flooding situation may be achieved by using more hydrophilic material as the bonder of the FTE and CME. In this case, it's more easily for KOH electrolyte to fill in the more hydrophilic pores. Thus, the real diffusion thickness for those pores that are completely flooded is much longer than the mean effective diffusion thickness 1 ~2 μm as estimated above because we cannot deduct the mass transport contribution through hydrophobic pores that are not flooded at all.

4. Results and discussion

4.1 Performance of the FTE and CME in a severe water-flooding situation

An experiment in which the both faces of the electrodes FTE and CME were entirely immersed in O_2-saturated KOH was designed to simulate severe flooding of oxygen electrodes, Figures 3 and 4 record chronopotentiometry of electrodes FTE and CME as dipped in 1 mol L^{-1} KOH, in which a gradually increased cathode current (Figure 3) and a constant cathode current (Figure 4) were imposed on the electrodes, respectively. Figure 5 records chronoamperometry of electrodes FTE and CME completely dipped in 1 mol L^{-1} KOH. Oxygen was fed at 10 mL min^{-1} near the back of the electrodes during the whole measurement.

With current flow through the electrode/electrolyte interface, the electrode potential will depart from the balance value. Electrode potential is going to shift toward the negative direction for cathode polarization and toward the positive direction for anode polarization. Figures 3, 4 and 5 tell us that, the FTE can sustain a larger polarization current (Figures 3 and

5) and a longer time at a fixed polarization current (Figure 4) than the CME can. It suggests that the DMS in the FTE can provide channels with higher O_2 transport through the liquid oil than through liquid water, and thus more O_2 is brought into the catalyst surface through the liquid oil than through liquid water. Figure 4 tells that the CME cannot sustain longer than 3 hours at polarization current density of 60 mA cm^{-2} before the electrode potential drops to -0.1 V. However, the FTE can sustain nearly 90 hours without obvious deterioration in electrode potential. The marked drop in electrode potential is a symbol of O_2 depletion in the electrode. With oxygen starvation, the cell reversal will soon appear in succession. Generally, at too high current densities, the electrode is going to be under mass transfer control, meaning that mass transport becomes the rate-determining step. The better flooding-tolerant capability of the FTE than the CME as they are completely dipped in KOH electrolyte is no doubt contributed to that for the FTE some of its channels filled by the liquid oil have higher O_2 transport but for the CME some of its channels filled by the liquid water have lower O_2 transport.

4.2 Half-cell tests

An experiment that can simulate the situation of a real half-cell in AFC and metal/air batteries is necessary for assessing electrode performance. There are two types of oxygen electrodes. One is made from PTFE-bonded catalysts, and the other from Nafion-bonded catalysts. The later was especially used to simulate a complete hydrophilic CME as reported after decomposition and partial removal of PTFE [1, 3, 6, 7, 9-12]. Poor mass transport of oxygen, which can be caused by low electrode porosity or by excessive wetting of the electrode, significantly increases polarization and reduces operating voltage. Generally, as

the current demand increases during operation, it is believed that the reaction front moves outward toward the air side of the electrode, and more of the electrode surface area participates in the reaction. The liquid electrolyte can film over or flood the electrode surface, thereby blocking oxygen access and reducing the available three-phase interfacial area for reaction. Therefore, compared with the CME, because the DMS in the FTE can supply the channels with higher O_2 transport through the liquid oil than through liquid water in the CME, the half-cell consisting of FTE cathode outputs higher cathode current density at a certain potential (Figure 6) or higher cathode potential (Figure 7) at a certain current density than the half-cell consisting of CME. Figure 6 indicates that the half-cell with CME cathode could output 1 A cm^{-2} current but the half-cell with FTE cathode as large as 1.5 A cm^{-2} as the half-cell potential jumps from 1.126 to 0.326 V. To fully demonstrate the flooding-tolerant capability of the FTE, we intentionally made the half-cell operate at a larger current density. In this case, the half-cell will suffer from the serious oxygen starvation and oxygen transport troubles. Of course, this will make the half-cells potential go down. Besides, the O_2 reduction reaction (ORR) on MnO_2 electro-catalysts undergoes a two-electron process to produce HO_2^- [38-42], thus, the use of low-cost MnO_2 electro-catalysts means a partial sacrifice of cathode potential relative to the direct four-electron process of ORR on noble metal of Pt [42]. Thus 1.5 A cm^{-2} and 1.0 A cm^{-2} of the current output for the half-cell with FTE or with CME is a quite large number in consideration of poor catalysis of MnO_2. Figure 7 discloses that with the gradual increase of cathode current, the cathode potential decline of the half-cell with FTE is not as steep as that of the cell with CME. At an acceptable current output, for example 0.4 A cm^{-2}, the electrode potential is 0.6 V for the half-cell with FTE but 0.47 V for CME.

Such an increase over 100 mV in voltage output of the half-cell is naturally assigned to the channels with higher O_2 transport through the liquid oil than through liquid water in company with DMS substituting for water.

In Figure 7, a gradually increased cathode current was imposed on the electrode with a time interval of 120 s. On the contrary, the polarization curves in Figure 8 are obtained by potentiodynamic scan with a scan rate of 2 mV s^{-1}. Therefore, it takes 20 min for the former but less than 10 min for the latter to finish the whole test. The flooding is getting more severe as an electrode is maintained at a larger current density for a long length of time [28]. That is why the performance of PTFE-bonded cathode, CME or FTE, seems not as good in Figure 7 as in Figure 8.

In addition, the differences in current density between the "PTFE-bonded CME" electrode and the "PTFE-bonded FTE" electrode shown in Figure 8 at a high cathode potential, for instance, 0.7 V, is not as great as that at low cathode potential, for instance, 0.3 V. It means that the performance improvement of the half-cell with FTE at small polarization is not as noticeable as at large polarization. The large polarization means the large current density and lower cathode potential. In this case mass transport is dominant over other processes. Thus, the half-cell with good mass transport cathode, such as FTE, will accordingly exhibit a better performance. However, at small polarization, the rate-determining step may be the electron transport step rather than the mass transfer step. Thus the measurement used for improving the mass transport would not improve the whole performance of the electrode.

Figures 9 and 10 are results based on the self-breathing cathodes. O_2 was fed at 60 mL

min^{-1} via the gas chamber as shown in Figure 2 before measurement and then stopped after measurement. The oxygen needed during experiment comes from (1) the oxygen stored in the pores of FTE and CME, and (2) air through the self-breathing of the cathode side exposed to the air. Figures 9 and 10 tell that more O_2 was stored in the FTE than the CME. The half-cell with FTE can sustain a larger polarization current (Figure 9) and longer time at a fixed polarization potential (Figure 10) than the CME in 1 mol L^{-1} KOH. It is worth noting that in comparison with the Nafion-bonded FTE, the PTFE-bonded FTE demonstrated much better catalysis to the ORR as shown in Figure 9. It is owing to the difference in hydrophobicity between PTFE and Nafion. The former is more hydrophobic but the latter less. The DMS is also hydrophobic. Thus, the pores in a PTFE-bonded FTE are more suitable for DMS storage than those of a Nafion-bonded FTE. Therefore there are more channels filled by the DMS in the PTFE-bonded FTE than in the Nafion-bonded FTE. In addition, Nafion-bonded FTE should be more easily subject to electrolyte penetration than the PTFE-bonded FTE. Therefore, more pores in Nafion-bonded FTE would be filled by KOH than in PTFE-bonded FTE. Thus, the PTFE-bonded FTE air electrode will own more oxygen transport channels and higher O_2 storage capacity than the Nafion-bonded FTE. And a better performance could be expected for the PTFE-bonded FTE.

Electrochemical impedance spectroscopy (EIS) of electrodes FTE and CME shown in Figure 11 further confirms the above analysis in another vision. The EIS analysis is used to resolve the frequency domain into the individual contributions of the various factors, ohmic, kinetic and mass transport. The small arcs at the high frequencies shown in Figure 11 are related to the outer electrode porosity over the electroactive region [43, 44] independent of

the applied potentials, which are in agreement with its ohmic nature. Then inverted deduction, if the whole real surface area of FTE is same as that of CME, the smaller arcs at the high frequency for the FTE imply that the electroactive region of FTE is larger than that of CME in the case of flooding, as a result compared with the CME the FTE can obtain a much larger polarization current, which is in agreement with the above analysis.

The diameter of the medium and partial low frequencies arcs in Figure 11 is referred to the polarization resistances (R_p), which is usually associated with the charge transfer across the electrode/electrolyte interface. However, if the time scale of the charge-transfer process is close to that of the slow oxygen diffusion processes responsible for the surface concentration of the electroactive species, R_p may contain contributions from all types of processes, which can be established through an analysis of the dependence of R_p on the cathode potential. In Figure 12, the cathode potential (half-cell voltage) was represented as a function of log R_p^{-1} following the eq. (3) [45].

$$V_{cath} = E_0 - b \log R_p^{-1} \quad (3)$$

The values of the intercept E_0 and slope b are obtained from the linear plots in Figure 12. There are two cases can be observed for the potential dependence of the resistance: (1) in a range of the high half-cell voltages (e.g. 0.826V to 0.726 V) the slopes of the straight lines is 0.12 and 0.13 V/decade for the CME and FTE, respectively, which implies that the oxygen diffusion is controlling the reaction kinetics [22] and should attribute to the agglomerate diffusion (the progressive depletion of oxygen within a pore) according to the thin-flim/flood-agglomerate model of gas diffusion electrodes developed by Raistrick [46,47]; (2) in a range of the low half-cell voltages (e.g. 0.626V to 0.426 V) the slopes of the straight

lines is 1.2 and 0.95 V/decade for the CME and FTE, respectively, which means the oxygen diffuses across an electrolyte film to the catalyst surface (thin film diffusion) [45,48]. Furthermore, the slope of the straight lines for the FTE is less than that for CME, which implies that FTE can obtain a higher cathode potential (half-cell voltage) than CME at the same condition.

At lower cathode potentials the electrode kinetics may be controlled by mass transfer, the main contribution of R_p comes from the oxygen diffusion resistance [49]. Therefore, the higher oxygen solubility in DMS extremely reduces the R_p of half-cell with FTE than that in CME at the same polarization potential. Moreover, the ratio of R_p^{CME}/R_p^{FTE} increases with the cathode potential decrease in a form of linear relation as shown in Figure 13. It means that the superiority capability of oxygen transfer and flooding-tolerant of FTE is more outstanding at lower cathode potential.

4.3 Distribution of the DMS in the FTE

Figure 14 shows the difference in pore volumes of a CME before and after introduction of the DMS. The main difference in pore volumes appears in the pores from 20 to 70 nm. It suggests that the DMS mainly fills in the pores with meso-diameter from 20 nm to 70 nm. It is the liquid electrolyte excessive condensation in the pores with a diameter from 20 to 70 nm that cause so-called flooding of the electrode. The pores with a diameter below 20 nm may always be occupied by water due to water capillary condensation in such small pores. The pores with a diameter over 70 nm may primarily belong to the gas, and water can be easily excluded by gas even though the large pores are occupied by water. Besides, due to the smaller capillary pressure in pores larger than 70 nm, it is slightly more difficult for water to

condense down in such large pores even though they become more hydrophilic owing to the PTFE degradation. The water in the pores with a diameter from 20 to 70 nm, however, may be not easily excluded because water capillary condensation in such pores is not as small as that in large pores. Therefore, the liquid electrolyte prefers to flood oxygen electrode via the pores with a diameter from 20 to 70 nm rather than that larger than 70 nm. The situation will be different if the pores with a diameter from 20 to 70 nm were in advance occupied by oil, such as DMS, which has a zero contact angle with carbon and Teflon, but 117° contact angle with water [50]. It can be expected that DMS can well penetrate into the pores configured by carbon and Teflon. Once the pores are occupied by DMS, the water-insoluble DMS is unlikely to be washed out of the electrode by product water.

It should be noted that we can't find any liquid medium which is better than void pores for oxygen transport. A compromising way is how to make the pathway of the oxygen transport as short as possible even though this pathway is filled by oil favorable to gas dissolution and transport. The DMS should be limited in the pores that are subject to water flooding rather than those void pores always belonging to gas phase, such as pores in the back layer of a porous electrode.

4 Conclusions

A more flooding-tolerant electrode (FTE) for the oxygen reduction reaction in alkaline was prepared by adding water-proof oil DMS into the conventional MnO_2/C electrode (CME). The FTE displays outstanding flooding-tolerant capability, especially in the case of a large current density, in which mass transport of reaction gas is in a dominant position. The success of FTE in flooding-tolerant is due to (1) DMS, in which the concentration of

dissolved oxygen is over 10 and 30 times higher than that in 1 mol L^{-1} KOH at 25 and 80 °C, respectively, supplies an channel with higher O_2 transport through the liquid oil than through liquid water and the higher solubility of oxygen in such DMS-filled channels as well as higher penetration of gaseous O_2 via the DMS into the electrode, (2) it partially mitigates the effects of water flooding to the catalyst layer of oxygen electrode used in AFC and metal/air batteries due to the PTFE degradation and physical wetting phenomenon in alkaline electrolyte and (3) it appears to provide an oxygen pathway through pores with a diameter of 20 to 70 nm, in which flooding often happens and is not easy to overcome.

Acknowledgements

This work was financially supported by NSFC of China (Grant Nos. 20476109, 20806096, 20936008 and 20906107), by program 863 of the Chinese Ministry of Science and Technology (Grant No. 2007AA05Z124), by Innovative Talent Training Project, Chongqing University (S-09013), and by Science Research Foundation of SKL-PES (2007DA10512708208).

References

[1]. M. Schulze, N. Wagner, T. Kaz, K. A. Friedrich, *Electrochim. Acta* **2007**, *52*, 2328.

[2]. M. Cifrain, K. V. Kordesch, *J. Power Sources* **2004**, *127*, 234.

[3]. P. Gouérec, L. Poletto, J. Denizot, E. Sanchez-Cortezon, J. H. Miners, *J. Power Sources* **2004**, *129*, 193.

[4]. E. Gülzow, N. Wagner, M. Schulze, *Fuel cells* **2003**, *3*, 67.

[5]. D. R. Sena, E. R. Gonzalez, E. A. Ticianelli, *Electrochim. Acta* **1992**, *37*, 1855.

[6]. N. Wagner, M. Schulze, E. Gülzow, *J. Power Sources* **2004**, *127*, 364.

[7]. M. Schulze, C. Christenn, *Appl. Surf. Sci.* **2005**, *252*, 148.

[8]. M. Schulze, M. Lorenz, T. Kaz, *Surf. Interf. Anal.* **2002**, *34*, 646.

[9]. M. Schulze, K. Bolwin, E. Gülzow, W. Schnurnberger, *Fresenius J. Anal. Chem.* **1995**, *353*, 778.

[10]. E. Gülzow, M. Schulze, *Degradation of nickel anodes during operation in alkaline fuel cells, in: Proceedings of the Fuel Cell Seminar*, Palm Springs, November, **2002**.

[11]. M. Schulze, E. Gu¨lzow, G. Steinhilber, *Appl. Surf. Sci.* **2001**, *179*, 251.

[12]. S. D. Song, H. M. Zhang, X. P. Ma, Z.-G. Shao, Y. N. Zhang, B. L. Yi, *Electrochem. Commun.* **2006**, *8*, 399.

[13]. M. Maja, C. Orecchia, M. Strano, P. Tosco, M. Vanni, *Electrochim. Acta* **2000**, *46*, 423.

[14]. G.-Q. Zhang, X.-G. Zhang, Y.-G. Wang, *Carbon* **2004**, *42*, 3097.

[15]. MA Al-Saleh, S Gultekin, AS Al-Zakri, H Celiker, *J. Appl. Electrochem.* **1994**, *24*, 575.

[16]. D. R. Lide, *Handbook of Chemistry and Physics* , *ed. 81st*, CRC Press, Boca Raton, FL, **2000–2001**, pp. 8–103.

[17]. K. V. Kordesch, *Brennstoffbatterien*, Springer–Verlag, Wien, New York, **1984**.

[18]. PD Michael, *An assessment of the prospects for fuel cell-powered cars*, ETSU, United Kingdom, **2000**.

[19]. K Kordesch, S Gunter,*Fuel cells and their applications*, Wiley-VCH, Berlin, Germany, **1996**.

[20]. AJ Appleby, FR Foulkes, *Fuel cell handbook*, Krieger Publishing Company, Malabar, Florida, **1993**.

[21]. G. F. McLean, T. Niet, S. Prince-Richard, N. Djilali, *Int. J. Hydrogen Energy* **2002**, *27*, 507.

[22]. H. Huang, W. K. Zhang, M. C. Li, Y. P. Gan, J. H. Chen, Y. F. Kuang, *J. Colloid Interface Sci.* **2005**, *284*, 593.

[23]. Ch.-Ch. Yang, S.-T. Hsu, W.-Ch. Chien, M. Ch. Shih, Sh.-J. Chiu, K.-T. Lee, Ch. L. Wang, *Int. J. Hydrogen Energy* **2006**, *31*, 2076.

[24]. M. Bursell, M. Pirjamali, Y. Kiros, *Electrochim. Acta* **2002**, *47*, 1651.

[25]. W. H. ZHU, B. A. POOLE, D. R. CAHELA, B. J. TATARCHUK, *J Appl Electrochem* **2003**, *33*, 29.

[26]. Y. Kiros, S. Schwartz, *J. Power Sources* **1991**, *36*, 547.

[27]. G. Velayutham, J. Kaushik, N. Rajalakshmi, K. S. Dhathathreyan, *Fuel cells* **2007**, *7*, 314.

[28]. E. Gülzow, *Fuel cells* **2004**, *4*, 251.

[29]. Z. D. Wei, W. Z. Huang, S. T. Zhang, J. Tan, *J. Power Sources* **2000**, *91*, 83.

[30]. D.J.G. Ives, G.J. Janz, *Reference Electrodes: Theory and Practice*, Academic Press, New York, **1961**.

[31]. S. M Xing, Y. L. Wang, *Synthetic Technics and Product Application of Organic Silicon*, Chemical Industry Press, Beijing, **2000**.

[32]. S.K. Shoor, R.D. Walker, K.E. Gubbins, *J. Phys. Chem.* **1969**, *73*, 312.

[33]. R.H. Li, *Elements of Mass Transfer*, Beijing Aviation College Press, Beijing, **1987**.

[34]. J. Giner, C. Hunter, *J. Electrochem. Soc.* **1969**, *116*, 1124.

[35]. A. J. Bard, L. R. Faulkner, *Electrochemical Methods*, Wiley & Sons, New York, **1980**.

[36]. I. Roche, E. ChaÎnet, M. Chatenet, J. Vondrák, *J. Phys. Chem. C* **2007**, *111*, 1434.

[37]. V. S. Murthi, R. C. Urian, S. Mukerjee, *J. Phys. Chem. B* **2004**, *108*, 11011.

[38]. M. L. Calegaro, F. H. B. Lima, E. A. Ticianelli, *J. Power Sources* **2006**, *158*, 735.

[39]. L. Q. Mao, D. Zhang, T. Sotomura, K. Nakatsu, N. Koshiba, T. Ohsaka, *Electrochim. Acta* **2003**, *48*, 1015.

[40]. F. H. B. Lima, M. L. Calegaro, E. A. Ticianelli, *J. Electroanal. Chem.* **2006**, *590*, 152.

[41]. T. Ohsaka, L. Q. Mao, K. Arihara, T. Sotomura, *Electrochem. Commun.* **2004**, *6*, 273.

[42]. L. Jörissen, *J. Power Sources* **2006**, *155*, 23.

[43]. F. Alcaide, E. Brillas, P.-L. Cabot, *J. Electroanal. Chem.* **2003**, *547*, 61.

[44]. S. Ahn, BJ. Tatarchuk, *J. Electrochem. Soc.* **1995**, *142*, 4169.

[45]. M. Ciureanu, R. Roberge, *J. Phys. Chem. B* **2001**, *105*, 3531.

[46]. T. E. Springer, I. D. Raistrick, *J. Electrochem. Soc.* **1989**, *136*, 1594.

[47]. I. D. Raistrick, *Electrochim. Acta* **1990**, *25*, 1579.

[48]. L. Genies, Y. Bultel, R. Faure, R. Durand, *Electrochim. Acta* **2003**, *48*, 3879.

[49]. L. Giorgi, E. Antolini, A. Pozio, E. Passalacqua, *Electrochim. Acta* **1998**, *43*, 3675.

[50]. R. H. Wu, M. J. Sun, *Surface and Interface of High Polymer*, Science Press, Beijing, **1998**.

Figure Captions

Fig. 1 Schematic diagram of anti-flooding in catalyst layer of conventional electrode (CME) and flooding-tolerant electrode (FTE).

Fig. 2 The structure of oxygen electrode and half-cell. (a) Two sides of oxygen electrode, (b) gold ring current collector, (c) rubber cushion, (d) Teflon holder, (e) gas chamber, (f) inlet and (g) outlet of gas reactant.

Fig. 3 Chronopotentiometry of electrodes Nafion-bonded FTE and CME under modulation of gradually increased current in O_2-saturated 1 mol L^{-1} KOH (O_2 fed at 10 mL min^{-1}).

Fig. 4 Chronopotentiometry of electrodes Nafion-bonded FTE and CPE at fixed cathode current of 60 mA cm^{-2} in O_2-saturated 1 mol L^{-1} KOH (O_2 fed at 10 mL min^{-1}).

Fig. 5 Chronoamperometry of electrodes Nafion-bonded FTE and CME as the electrode potential jumps from 1.126 to 0.326 V in O_2-saturated 1 mol L^{-1} KOH (O_2 fed at 10 mL min^{-1}).

Fig. 6 Chronoamperometry of half-cell with cathodes PTFE-bonded FTE and CME as cathode potential jumps from 1.126 to 0.326 V in 1 mol L^{-1} KOH (O_2 fed at 60 mL min^{-1}).

Fig. 7 Chronopotentiometry of half-cell with cathodes PTFE-bonded FTE and CME as cathode under modulation of gradually increased current in 1 mol L^{-1} KOH (O_2 fed at 60 mL min^{-1}).

Fig. 8 Cell voltage vs. Current density of a half-cell with cathodes CME and an FTE as cathode at scan rate of 2 mV s^{-1} in 1 mol L^{-1} KOH (O_2 fed at 60 mL min^{-1}).

Fig. 9 Cell voltage vs. Current density of a half-cell with cathodes CME and an FTE as cathode at scan rate of 2 mV s^{-1} in 1 mol L^{-1} KOH (Air self-breathing).

Fig. 10 Chronopotentiometry of a half-cell with cathodes PTFE-bonded FTE and CME as cathode under modulation of gradually increased current in 1 mol L^{-1} KOH (Air self-breathing).

Fig. 11 Potential dependence of the Nyquist plots obtained for an half-cell with cathodes Nafion-bonded FTE and CME as cathode in 1 mol L^{-1} KOH (1×10^{4} to 1×10^{-2} Hz; O_2 fed at 60 mL min^{-1}).

Fig. 12 Cathode potential vs $\log(R_p^{-1})$ for an half-cell with Nafion-bonded CME and Nafion-bonded FTE in 1 mol L^{-1} KOH (O_2 fed at 60 mL min^{-1}).

Fig. 13 R_p ratio of Nafion-bonded CME to Nafion-bonded FTE as a function of the cathodic potential for an half-cell in 1 mol L^{-1} KOH (O_2 fed at 60 mL min^{-1}).

Fig. 14 Change in pore volume of a CME before and after addition of 2.5 mg cm^{-2} DMS (the CME has apparent area of 4 cm^2).

Table

Table 1 Oxygen diffusion limiting current densities i_l (mA cm^{-2}) of the ORR vs the effective diffusion thickness L in the liquid phase of the catalyst layer (170 μm) at 25 and 80 °C, respectively.

L / μm	0.1		0.2		0.5		0.8		1.0		1.5		2.0	
°C	25	80	25	80	25	80	25	80	25	80	25	80	25	80
CME	465	165	232.5	82.5	93	33	58	20.6	46.5	16.5	31	11	22.3	8.2
FTE	3000	3000	1500	1500	600	600	375	375	300	300	200	200	150	150

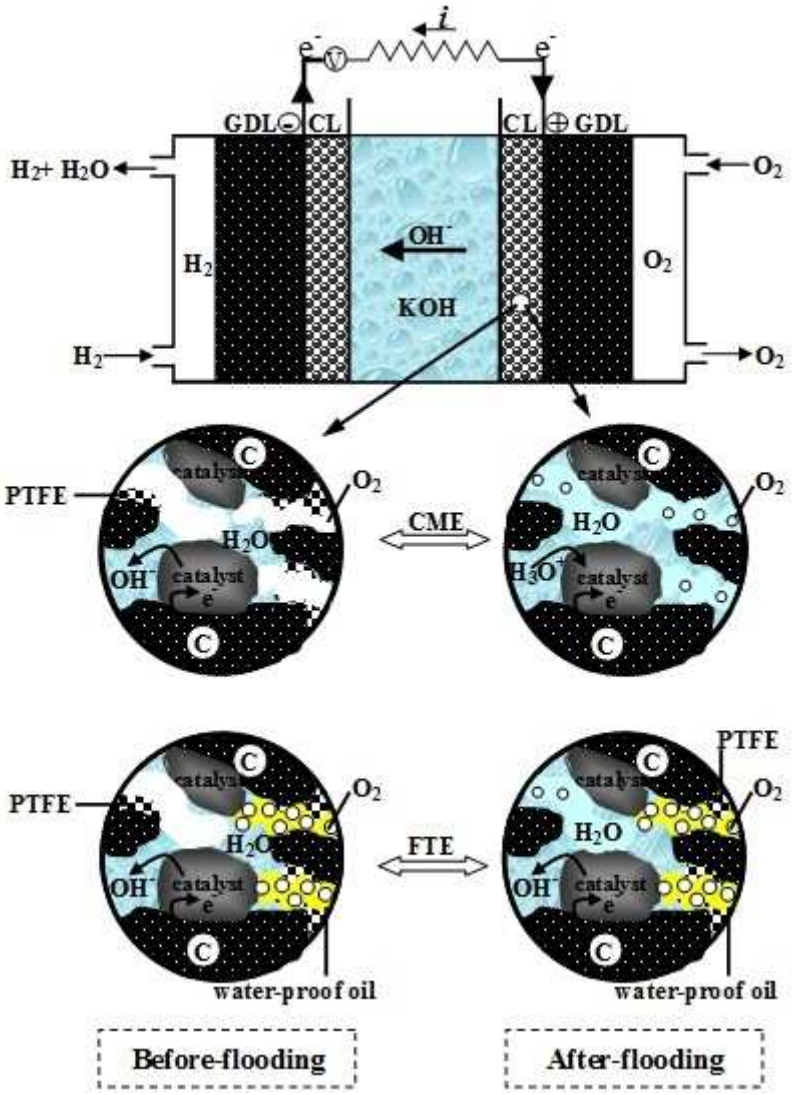

151x194mm (72 x 72 DPI)

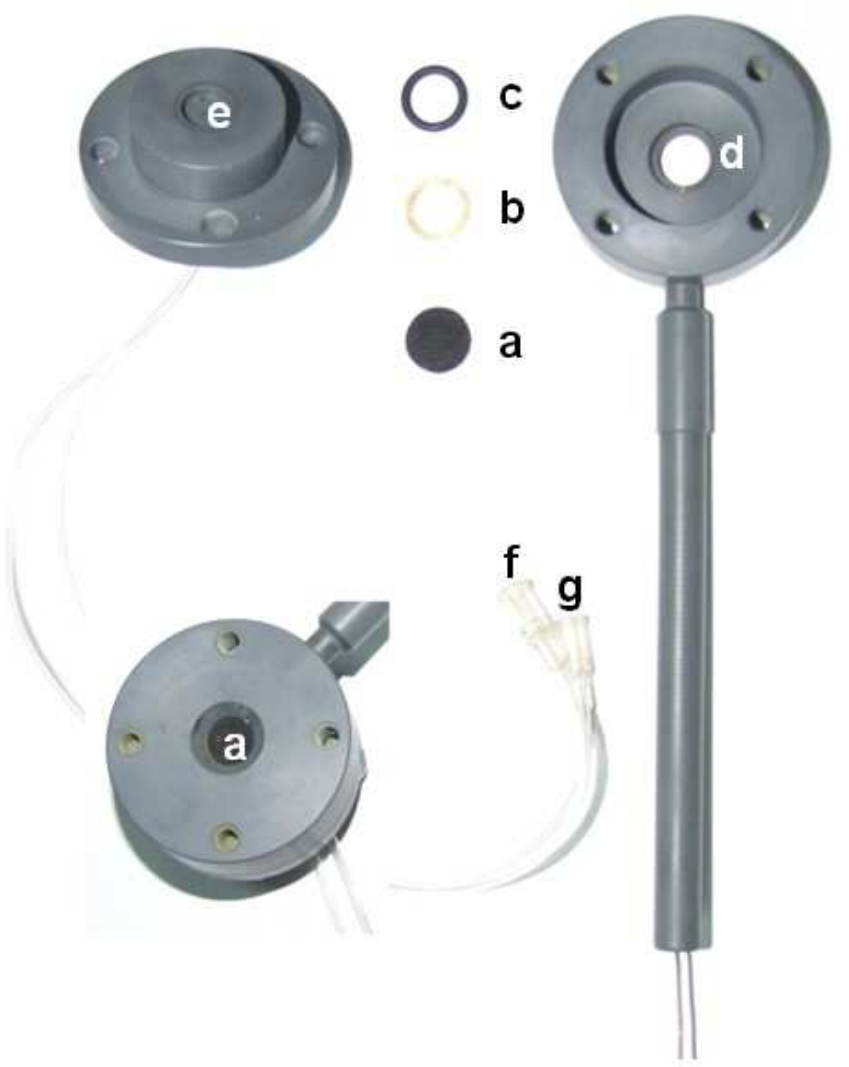

192x213mm (72 x 72 DPI)

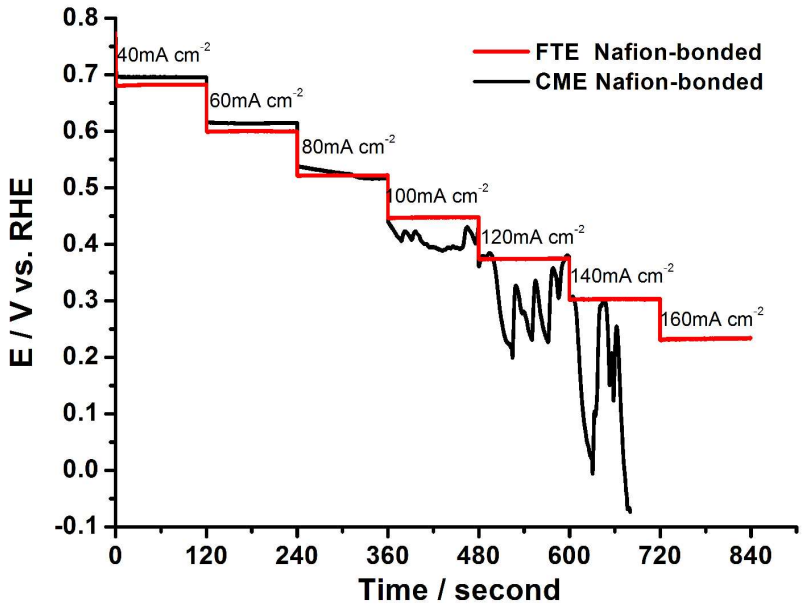

297x210mm (300 x 300 DPI)

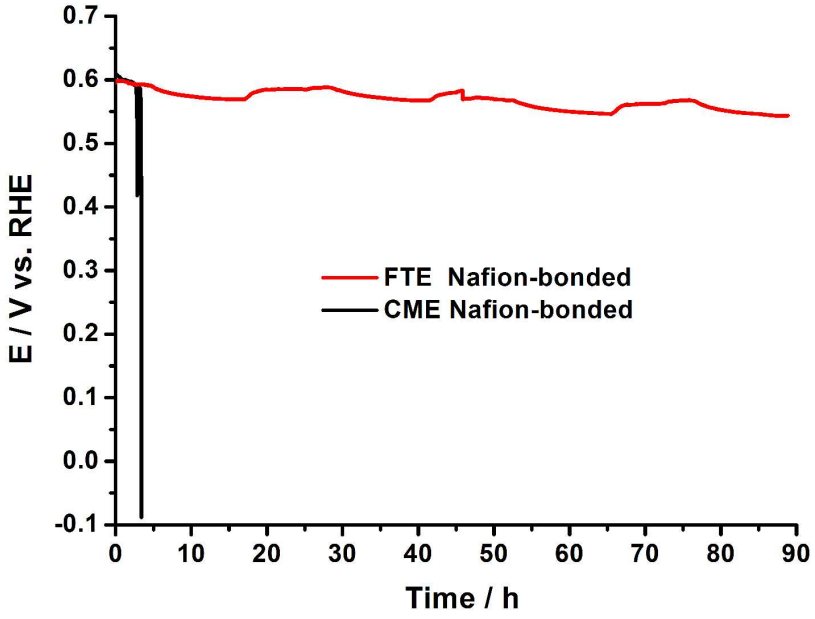

297x210mm (300 x 300 DPI)

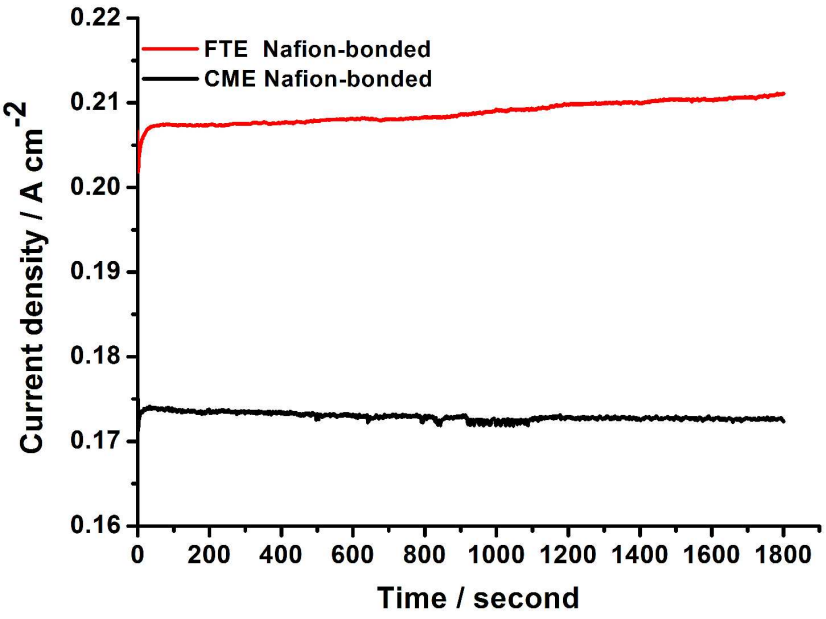

297x210mm (300 x 300 DPI)

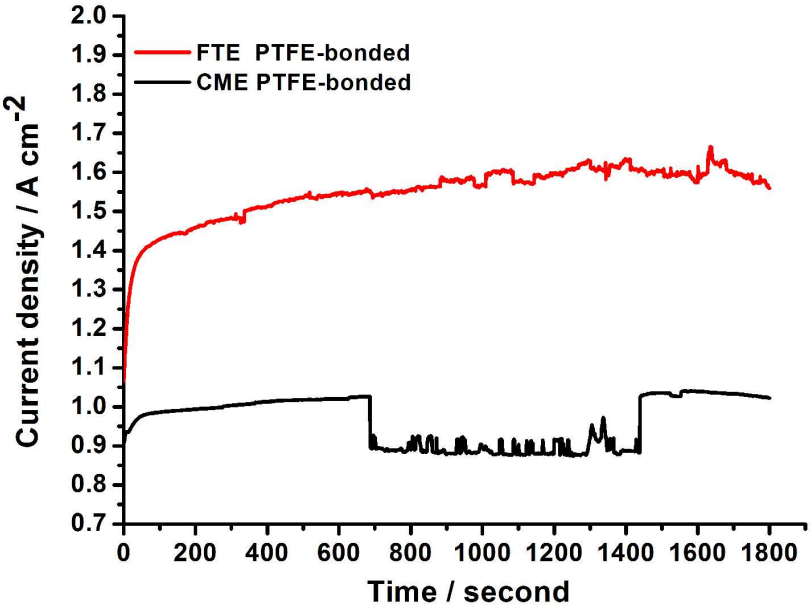

297x210mm (300 x 300 DPI)

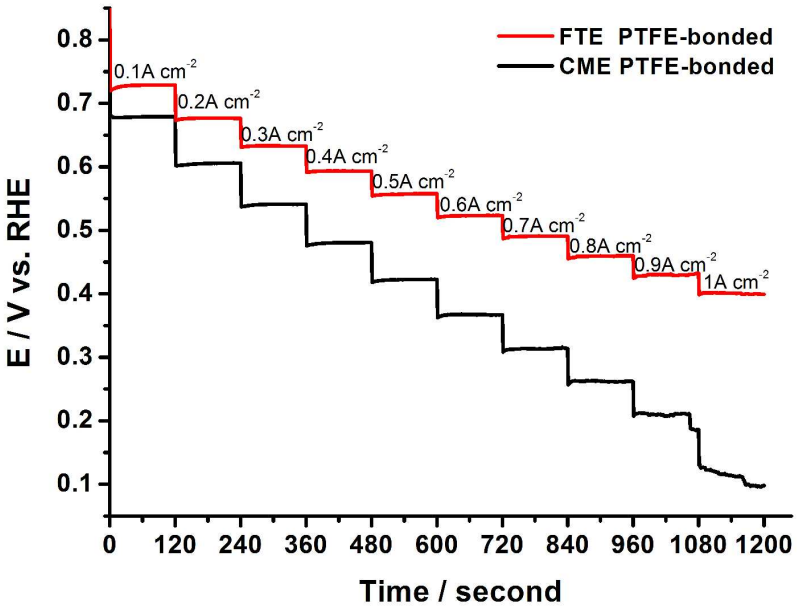

297x210mm (300 x 300 DPI)

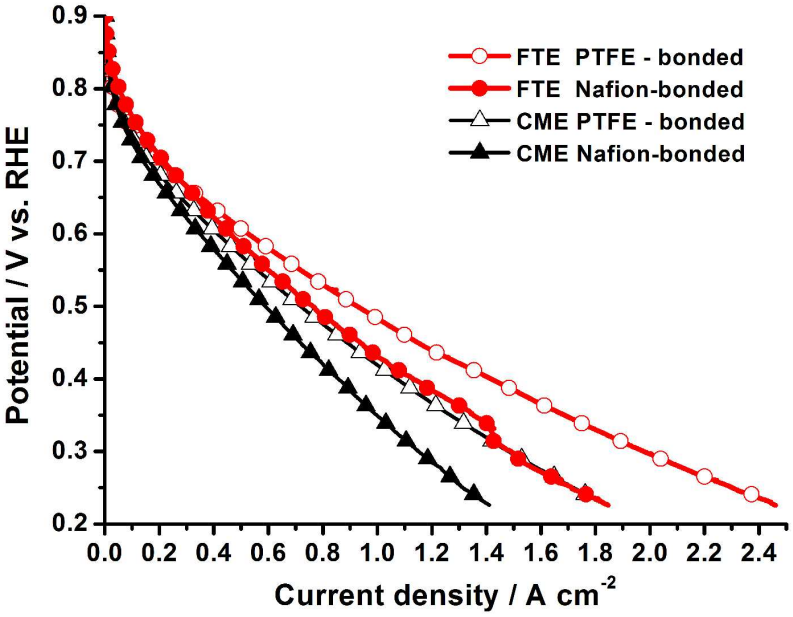

297x210mm (300 x 300 DPI)

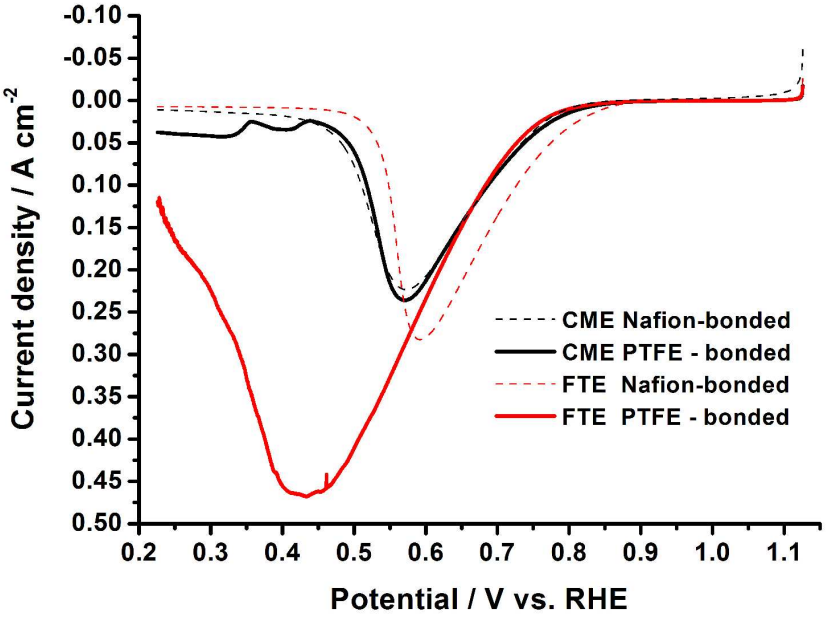

297x210mm (300 x 300 DPI)

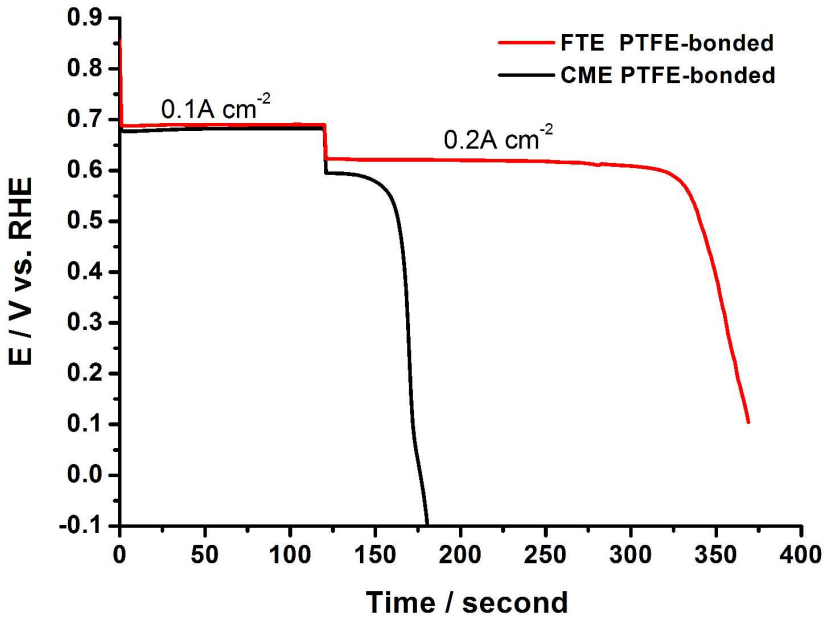

297x210mm (300 x 300 DPI)

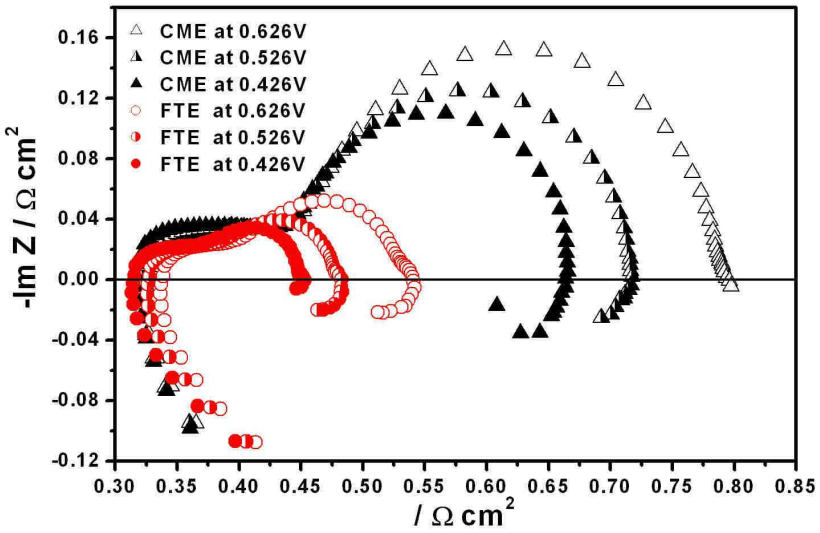

296x209mm (150 x 150 DPI)

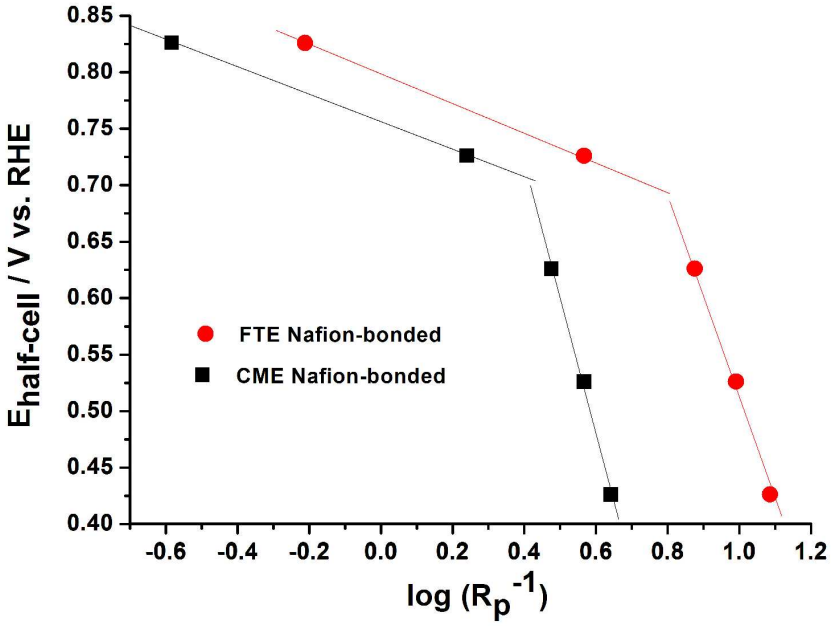

297x210mm (300 x 300 DPI)

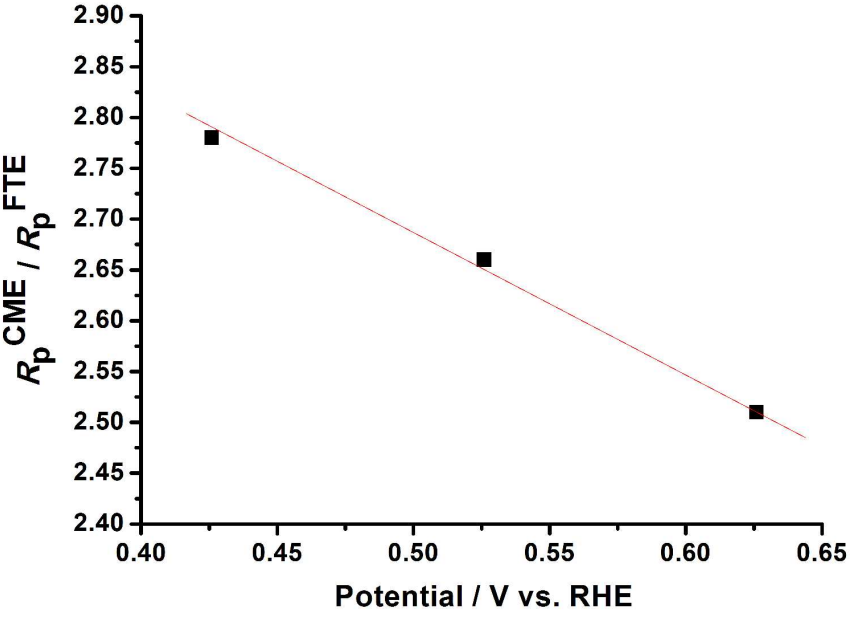

297x210mm (300 x 300 DPI)

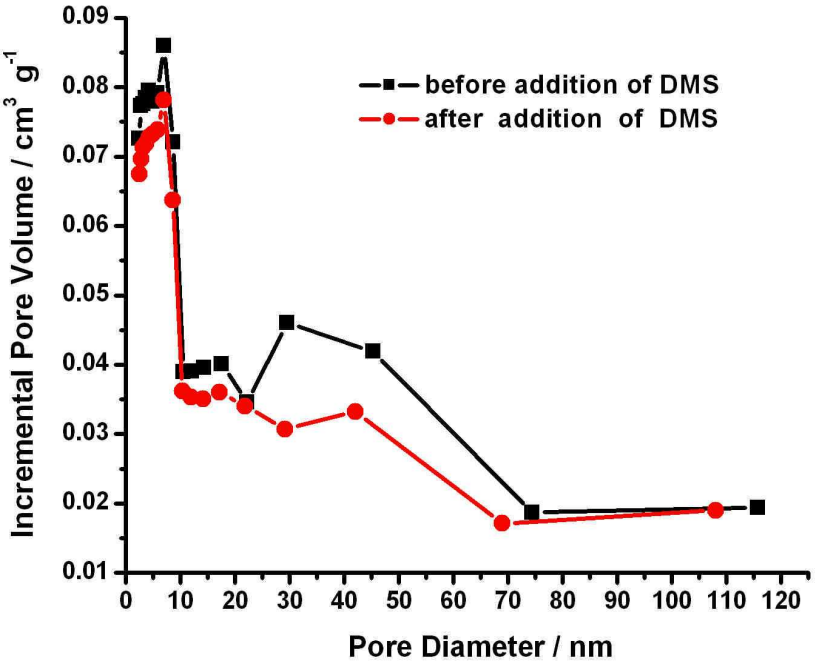

279x215mm (150 x 150 DPI)